

# Efficiency of the coherent biexciton admixture mechanism for multiple exciton generation in InAs nanocrystals

**Piotr Kowalski, Paweł Machnikowski**

Department of Theoretical Physics, Wrocław University of Technology, 50-370 Wrocław, Poland

E-mail: [pawel.machnikowski@pwr.edu.pl](mailto:pawel.machnikowski@pwr.edu.pl)

**Abstract.** We study the coherent mixing between two-particle (single exciton) and four-particle (biexciton) states of a semiconductor nanocrystal resulting from the coulomb coupling between states with different numbers of electron-hole pairs. Using a simple model of the nanocrystal wave functions and an envelope function approach, we estimate the efficiency of the multiple exciton generation (MEG) process resulting from such coherent admixture mechanism, including all the relevant states in a very broad energy interval. We show that in a typical ensemble of nanocrystals with 3 nm average radius, the onset of the MEG process appears about 1 eV above the lower edge of the biexciton density of states and the efficiency of the process reaches 50% for photon energies around 5 eV. The MEG onset shifts to lower energies and the efficiency increases as the radius grows. We point out that the energy dependence of the MEG efficiency differs considerably between ensembles with small and large inhomogeneity of nanocrystal sizes.

## 1. Introduction

Confining the carriers to a nanometer-scale volume of a semiconductor nanostructure not only leads to qualitative modification of the energy spectrum but also changes the relative role of various kinetic processes that take place in these systems. In particular, it has been proposed [1] that an enhancement of impact ionization processes in nanostructures can be exploited to increase the efficiency of solar cells by enabling multiple exciton generation (MEG) upon absorption of a single high-energy photon. In spite of the initial controversy concerning the actual efficiency of this process [2, 3, 4, 5, 6, 7], which arise from the experimental difficulty in extracting the real MEG yields [8, 9, 10], direct measurements of photocurrent from nanocrystal-based structures [11, 12] confirm the initial expectation that efficiency enhancement due to the MEG process is feasible.

In the single-particle picture, only the transitions leading to creation of a single electron-hole pair (exciton) are optically active. Therefore, the MEG process requires Coulomb interactions that couple configurations with different numbers of excitons. Such inter-band Coulomb couplings are indeed present in semiconductor nanocrystals and can be theoretically computed by various methods [13, 14, 15, 16, 17, 18, 19, 20, 21, 22, 23, 24]. In their presence, there are various scenarios that can lead to the MEG effect. For instance, one can think of a sequential process in which the initially created high-energy exciton subsequently decays into the biexciton states that form a quasi-continuum with very high density of states at sufficiently high energies. The rates for such a process have been calculated using atomistic methods [16, 13, 14]. On the other hand, biexciton states can be created coherently due to the Coulomb-induced mixing between the single-exciton (X) and biexciton (BX) states [25, 26]. In this picture, admixture of BX states to X states increases the average number of excitons in the resulting few-particle eigenstate, while admixture of certain X states to BX states can make the latter optically active. As a result, the nanocrystal state emerging from a single photon absorption can involve more than one electron-hole pair on the average.

In this paper, we estimate the efficiency of MEG resulting from the admixture mechanism in an InAs nanocrystal. We use the method for calculating the Coulomb couplings between X and BX states based on the envelope function ( $\mathbf{k} \cdot \mathbf{p}$ ) approach developed in our previous paper [25], which is a low-cost approximate method that allows us to build statistics over very many X and BX states in a broad energy window and for a distribution of nanocrystal sizes. The predicted efficiencies are in the range of several up to 50% for photon energies below 5 eV, which is roughly consistent with experimental findings [27, 9].

The paper is organized as follows. In Sec. 2, we present the model and the method used to estimate the efficiencies. The results are discussed in Sec. 3. Sec. 4 concludes the paper.

## 2. Model and method

We use the simple model of a spherical nanocrystal as in Ref. [25]. The carrier states are modeled by single-band wave functions with envelopes corresponding to a simple spherical potential well with infinite barriers, with a constant hole effective mass and a self-consistent, energy-dependent electron mass [28, 25]. Thus, each single particle state is characterized by the band and the three quantum numbers  $(n, l, m)$  for the envelope wave function. Two kinds of few-particle configurations are relevant here:

The first group are optically active (bright) states with one electron-hole (e-h) pair, referred to as single exciton (X) states. In our model, for such states to be bright (in the sense of a dipole-allowed transition), the quantum numbers  $n, l$  of the electron and the hole must be the same, while the values of  $m$  must be opposite. In addition, the band angular momentum (“spin”) projection of the hole must be specified to fully characterize the state. Only the states with holes from the  $j = 3/2$  valence band can be bright. The second group are states with two e-h pairs, referred to as biexciton (BX) states. These are labeled by the full set of quantum numbers for the two electron and two hole states, as well as the spin (singlet-triplet) configuration of the two electrons and the subband (“spin”) configuration of the two holes.

Only the diagonal (first order) Coulomb correction to the energies of X and BX states as well as the electron and hole exchange energies for the BX states are taken into account. This is done on the usual mesoscopic level of envelope functions. In addition, the intraband Coulomb coupling (i.e., coupling between configurations with a different number of e-h pairs), which is relevant for the effect to be discussed here, is included. On the mesoscopic level, these Coulomb terms vanish in the single band approximation due to orthogonality of Bloch functions [25, 26], hence they are taken on the microscopic level involving the Bloch functions, in the first order of the expansion in terms of  $a/R$ , where  $a$  is the lattice constant and  $R$  is the nanocrystal radius (see Refs. [25, 26] for details). All the Coulomb couplings taken into account include both the direct interaction term as well as interaction mediated by surface polarization which is due to the dielectric discontinuity on the nanocrystal border. Here we only include couplings corresponding to creation of an e-h pair with electron intraband relaxation, with the other hole being a “spectator”. The values of all the parameters, corresponding to an InAs nanocrystal, are as in Ref. [25].

An inhomogeneous ensemble of nanocrystals is modeled by assuming a Gaussian distribution of nanocrystal radii  $f(R)$ , with the average  $R_0$  and standard deviation  $\sigma_R$ . In practice, the size dependence of the Coulomb couplings is given by a simple  $1/R$  or  $1/R^2$  scaling [25], while the energies have been computed for 7 values of  $R$  in the range (2.7, 3.3) meV and approximated by a quadratic fit, which yields a good quantitative approximation in the required range of nanocrystal radii.

The BX admixture to an X state  $|X_j\rangle$  in a nanocrystal of a given radius is obtained (as in Ref. [25]) by diagonalizing the Hamiltonian including only the X state in question and the BX states  $|BX_i\rangle$  directly and sufficiently strongly coupled to  $|X_j\rangle$ . The criterium for the selection of these “sufficiently strongly coupled” BX states out of the infinite number of such states is as follows: If  $h_{ji}$  is the magnitude of the coupling matrix element between the two states and  $\Delta E_{ji}$  is the energy separation between them, then a given state BX is included if the ratio  $q_{ji} = |h_{ji}/\Delta E_{ji}|$  is larger than 0.01. Note that  $|q_{ji}|^2$  is the perturbative measure of the admixture of a given state BX to X. After diagonalization of the Hamiltonian constructed in this way, we select the eigenstate  $|\Psi_0^{(j)}\rangle$  with the highest X contribution as the new nominally single-exciton state and its BX admixture is determined as

$$x_{\text{BX/X}}^{(j)} = \sum_i \left| \langle BX_i | \Psi_0^{(j)} \rangle \right|^2 = 1 - \left| \langle X_j | \Psi_0^{(j)} \rangle \right|^2.$$

In the calculation of the MEG efficiency as a function of the photon energy, we need the relative absorption by a given state and the resulting number of e-h pairs. For a nominally single-exciton state, the former is proportional to the brightness

$S_j = (1 - x_{\text{BX}/\text{X}}^{(j)})s_j$  of this state, where the nominal brightness  $s_j = 1$  for a heavy-hole exciton and  $s_j = 1/3$  for a light-hole exciton. The contribution of this state to the overall absorption of an inhomogeneous ensemble is  $f(R)S_j$ . On the other hand, its relative contribution to the e-h pair production is  $f(R)S_j(1 + x_{\text{BX}/\text{X}}^{(j)})$ .

The X admixture to bright BX states is determined in a similar way. We diagonalize the Hamiltonian containing only the BX state in question (denoted  $|BX_j\rangle$ ) and all the bright X states  $|X_i\rangle$  directly and sufficiently strongly coupled to the BX state (those for which  $q \geq 0.01$ ). We identify the eigenstate  $|\Phi_0^{(j)}\rangle$  which has the biggest BX component and treat it as the new, corrected BX state. The single-exciton admixture to this state is equal to

$$x_{\text{X}/\text{BX}}^{(j)} = 1 - \left| \langle BX_j | \Phi_0^{(j)} \rangle \right|^2.$$

The brightness of the BX states is  $S_j = \sum_i x_{\text{X}/\text{BX}}^{(ji)} s_i$ , where  $x_{ji}$  and  $s_i$  are the admixtures of various X states and their nominal brightness, respectively (in the vast majority of cases, there is only one sufficiently strongly coupled X state). The relative contribution to the absorption is  $f(R)S_j$  and the relative contribution to the e-h pair production is  $f(R)S_j(2 - x_{\text{X}/\text{BX}}^{(j)})$ .

In practice, since the largest Coulomb couplings found for our model of the nanocrystal with a 3 nm radius are around 40 meV, we include admixed states with energies up to 10 eV (in the whole relevant range of radii) in order to provide quantitatively correct results in the 5 eV energy range of interest.

We then simulate an inhomogeneous nanocrystal ensemble by sampling the radius distribution at 0.003 nm intervals and compute the dependence of the MEG efficiency on energy as a histogram with the energy axis divided into finite bins of  $\delta E = 20$  meV width. In the energy bin  $l$  with a central energy  $\mathcal{E}_l$ , the total absorption rate is calculated (up to a constant factor) as

$$\alpha_l = \sum_{nj} f(R_n) S_j(R_n) \Theta(\delta E/2 - |\mathcal{E}_l - E_j(R_n)|),$$

where  $n$  numbers the nanocrystals in the simulated ensemble,  $j$  runs through all the X and BX states,  $\Theta$  is the Heavyside step function, and we have explicitly written the  $R$ -dependence of the energy and brightness of the state  $j$ . The e-h pair production rate is

$$\begin{aligned} \beta_l &= \sum'_{nj} f(R_n) S_j(R_n) (1 + x_{\text{BX}/\text{X}}^{(j)}) \\ &\quad \times \Theta(\delta E/2 - |\mathcal{E}_l - E_j(R_n)|) \\ &\quad + \sum''_{nj} f(R_n) S_j(R_n) (2 - x_{\text{X}/\text{BX}}^{(j)}) \\ &\quad \times \Theta(\delta E/2 - |\mathcal{E}_l - E_j(R_n)|), \end{aligned}$$

Where the first sum runs through the X states and the second one through the BX states. The MEG efficiency is then

$$F(\mathcal{E}_l) = \frac{\beta_l}{\alpha_l} - 1,$$

that is,  $F = 1$  corresponds to 100% biexciton generation.

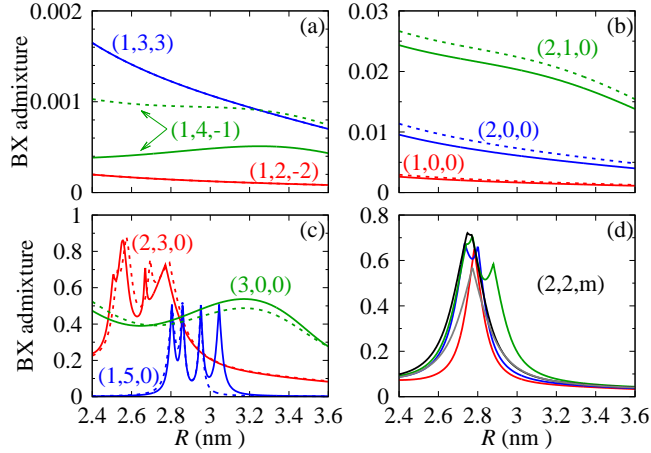


**Figure 1.** Admixture of BX states to bright X states as a function of the nanocrystal radius. The states are labeled by their quantum numbers  $n, l, m$ . Solid (dashed) lines correspond to excitons with the hole spin projections of  $\pm 3/2$  and  $\pm 1/2$ , respectively. In (a,b) selected low-energy states are shown. In (c,d) we show some states of higher energy.

### 3. Results

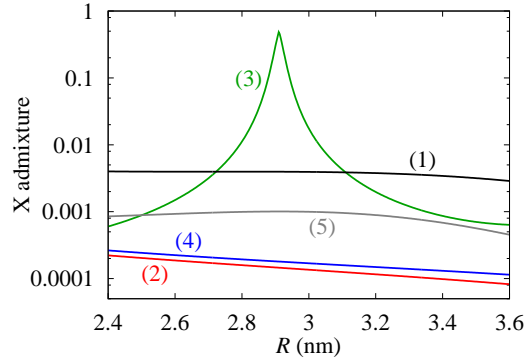
We begin the discussion of the results from an overview of the typical values of X and BX admixtures to the BX and X states, respectively, as well as their dependence on the nanocrystal radius.

In Fig. 1(a,b) we show the BX admixture to a few selected low-energy states (the exact information on the energies is contained in the Appendix) as a function of the radius  $R$ . The value of this admixture remains very low even for states up to 1 eV above the lowest BX state, which is due to selection rules that exclude coupling between excited bright X states and the lowest BX states [25]. The admixture to X states with  $\pm 1/2$  hole spin projection is typically slightly higher than to those with  $\pm 3/2$  hole spin.

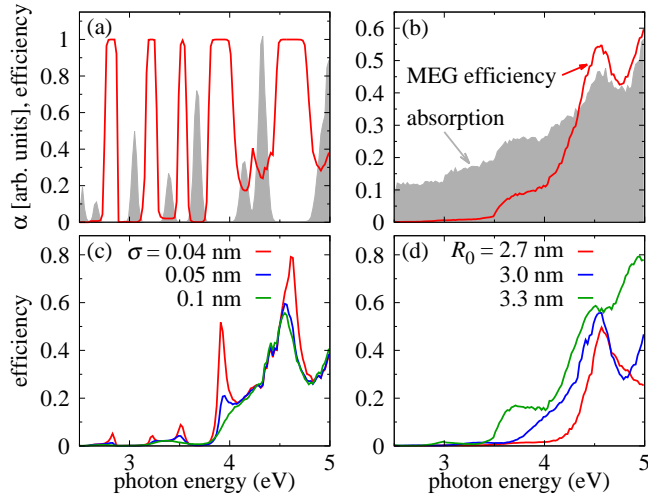
Fig. 1(c,d) presents the BX admixture for selected states with higher energies. In general, much higher values are obtained in this case. The  $R$  dependence clearly has a resonant character and peaks for some nanocrystal radii, when the coupled X and BX states cross. As shown in Fig. 1(c,d), there is only very weak dependence on the value of the quantum number  $m$  and on the hole spin projection in the X state.

Fig. 2 shows the admixture of X states to BX states. In most cases, this value does not exceed 0.01, irrespective of the energy of a given BX state (see Appendix for detailed information on the states selected for this figure) hence these states remain nearly completely dark. However, as illustrated by the case (3) in Fig. 2, resonant enhancement of the admixture may happen in the case of a resonance between the chosen BX state and one of the X states. Then, in a relatively narrow peak, admixture reaches 0.5. In spite of the large number of states sufficiently strongly coupled to one of the bright states with energy below 5 eV (about 7500 BX states for  $R = 3$  nm in our model), there are only several tens of such resonances in this energy window.

Finally, Fig. 3 shows the dependence of the MEG efficiency on the photon energy. In a nearly homogeneous ensemble of nanocrystals (Fig. 3(a)), the efficiency reaches



**Figure 2.** X admixture to selected BX states.



**Figure 3.** The MEG efficiency (lines) as a function of the photon energy: (a) for a very weakly inhomogeneous ensemble ( $R_0 = 3$  nm,  $\sigma = 0.02$  nm), compared with the absorption coefficient (shaded area); (b) as in (a) but for a much larger ensemble inhomogeneity ( $\sigma = 0.3$  nm); (c) as a function of the inhomogeneity for  $R_0 = 3$  nm; (d) as a function of the average radius for  $\sigma = 0.15$  nm.

1 in certain energy intervals. Comparison with the absorption spectrum shows that this happens only for energies where absorption is nearly absent. Clearly, the reason for such an efficient biexciton generation is the discrete nature of the single exciton density of states: in a weakly inhomogeneous ensemble there are extended energy intervals where no bright single exciton states are present so that all the absorption originates from the quasi-continuous background of nearly purely biexcitonic states.

This picture is different in an ensemble of nanocrystals with a broader size distribution (Fig. 3(b)). Now both the absorption and the MEG efficiency become quasi-smooth functions of the photon energy and both grow nearly monotonically. The onset of the MEG (the MEG threshold) is clearly marked at 3.5 eV, which should be contrasted with the nominal onset of the BX density of states at  $\sim 2.5$  eV for

$R = 3$  nm.

The evolution of the energy dependence of the MEG efficiency with increasing inhomogeneity is shown in more detail in Fig. 3(c). Here one can see that already at  $\sigma = 0.04$  nm the overlap of the inhomogeneously broadened absorption peak is sufficient to suppress the large values of the efficiency, leaving only a few marked maxima. These MEG efficiency peaks are then washed out as the inhomogeneity grows further.

In Fig. 3(d) we show the MEG efficiency for three ensembles with different average nanocrystal radii. The two features that can be noticed are the a shift of the MEG threshold towards lower energies and larger overall values of the MEG efficiency for larger nanocrystals.

#### 4. Conclusions

We have estimated the quantum efficiency of the multiple exciton generation via coherent, Coulomb-induced mixing of bright exciton and biexciton states. Although the mixing is, in general, rather weak due to small values of the Coulomb coupling elements (not exceeding a few tens of meV), it can become much stronger near the crossing point between the X and BX energies at particular values of the nanocrystal radius. The relatively low computational cost of the envelope function method used in our calculations has allowed us to include all the relevant states in a 10 eV energy window.

An interesting property that emerges from our calculations is the high MEG yield in the energy intervals where the single exciton density of states vanishes in a weakly inhomogeneous ensemble. Although this result has been obtained in our simple model of nanocrystal wave functions, it essentially follows from the discrete nature of single-exciton spectrum for moderate energies and the much more dense, quasi-continuous spectrum of biexciton states. Therefore, it should be a general feature of highly homogeneous nanocrystal ensembles. Whether this can be exploited in applications depends on the technological feasibility of building a structure in which the very weak absorption of biexciton states is accumulated to yield a considerable overall carrier injection.

In contrast, for less homogeneous nanocrystal ensembles, both the absorption and MEG efficiency are smooth functions of the photon energy, with a threshold at about 3.5 eV for nanocrystals with 3 nm radius, which is 1 eV above the formal onset of the biexciton density of states. The threshold shifts to lower energies for larger nanocrystals. The efficiencies of the MEG process reach 50% for the photon energies about 5 eV and average radius of 3.0 nm and increase for larger nanocrystals.

#### Appendix A. Information on the states used in the figures

In this appendix we present the detailed information about the states shown in Fig. 1 and Fig. 2.

Table A1 shows the energies of all the bright single exciton states with energies below 5 eV at  $R = 3$  nm. The values are shown for three nanocrystal radii. In our model, bright states are those with identical quantum numbers  $n, l$  for the electron and the hole (shown in the leftmost columns). Shifts induced by mixing with different BX states lead to differences between the energies of X states with different values of  $m$  as well as between states with different projections of the hole spin. However,

state		energy (eV)		
$n$	$l$	$R = 2.4$ nm	$R = 3.0$ nm	$R = 3.6$ nm
1	0	1.59	1.30	1.11
1	1	2.34	1.86	1.57
1	2	3.11	2.45	2.03
1	3	3.92	3.05	2.51
1	4	4.77	3.67	3.00
1	5	5.66	4.32	3.52
2	0	3.41	2.67	2.21
2	1	4.39	3.39	2.78
2	2	5.41	4.14	3.37
2	3	6.47	4.91	3.97
3	0	5.66	4.31	3.50

**Table A1.** Energies of single exciton states for three values of the nanocrystal radius.

	state						energy (eV)		
	e	e	h	h	$\Sigma_e$	$\Sigma_h$	2.4 nm	3.0 nm	3.6 nm
(1)	100	100	$21\bar{1}$	200	$S$	$T_0^{(3/2)}$	4.66	3.56	2.92
(2)	111	100	210	110	$T_+$	$S_{\uparrow\downarrow}$	4.87	3.87	3.13
(3)	100	100	151	$14\bar{1}$	$S$	$S_{\uparrow\downarrow}$	5.78	4.31	3.47
(4)	210	100	$21\bar{1}$	110	$S$	$T_+^{(1/2)}$	6.21	4.84	4.01
(5)	121	100	230	$12\bar{2}$	$T_0$	$S$	6.55	4.96	4.02

**Table A2.** Quantum numbers, spin configurations, and energies of biexciton states used in Fig. 2. Labels (1)–(5) refer to that figure.

these differences are very small, within 10 meV, hence we show only the energies of the state with 3/2 hole spin projection and  $m = 0$ .

Table A2 shows the full data on the states presented in Fig. 2. Here the first four columns contain the quantum numbers  $nlm$  for the two electrons and the two holes (negative values of  $m$  are denoted by a bar over the number) and the next two columns show the spin configurations: For the electron, this is just singlet ( $S$ ) or one of the three triplet states ( $T_{0,\pm}$ ) with the total spin projection 0 or  $\pm 1$ . For two-hole states with both holes with  $\pm 3/2$  or with both holes with  $\pm 1/2$  spin projection, the basis configurations are also singlet or triplet, with the additional upper index (3/2) or (1/2), respectively. In addition, configurations in which one hole has a 1/2 spin projection and the other one has 3/2 spin projection appear in our calculations. For these, we introduce the symmetrized and antisymmetrized spin states, denoted  $S_{\uparrow\uparrow}$ ,  $A_{\uparrow\uparrow}$ , etc, where thin and thick arrows correspond to hole states with the angular momentum projection 1/2 and 3/2, respectively. The final three columns show the energies of the state for three radii of a nanocrystal, as in the previous table.

## References

- [1] Nozik A J 2002 *Phys. E* **14** 115
- [2] Schaller R D, Agranovich V M and Klimov V I 2005 *Nat. Phys.* **1** 189–194



- [3] Schaller R D, Sykora M, Pietryga J M and Klimov V I 2006 *Nano Lett.* **6** 424–429
- [4] Schaller R D, Pietryga J M and Klimov V I 2007 *Nano Lett.* **7** 3469–3476
- [5] Trinh M T, Limpens R, de Boer W D A M, Schins J M, Siebbeles L D A and Gregorkiewicz T 2012 *Nat. Photonics* **6** 316
- [6] Nair G and Bawendi M G 2007 *Phys. Rev. B* **76** 81304
- [7] Ben-Lulu M, Mocatta D, Bonn M, Banin U and Ruhman S 2008 *Nano Lett.* **8** 1207
- [8] Pijpers J J H, Hendry E, Milder M T W, Fanciulli R, Savolainen J, Herek J L, Vanmaekelbergh D, Ruhman S, Mocatta D, Oron D, Aharoni A, Banin U and Bonn M 2007 *J. Phys. Chem. C* **111** 4146–4152
- [9] McGuire J A, Sykora M, Joo J, Pietryga J M and Klimov V I 2010 *Nano Lett.* **10** 2049–2057
- [10] Binks D J 2011 *Phys. Chem. Chem. Phys.* **13** 12693
- [11] Sambur J B, Novet T and Parkinson B A 2010 *Science* **330** 63–66
- [12] Semonin O E, Luther J M, Choi S, Chen H Y, Gao J, Nozik A J and Beard M C 2011 *Science*, **334** 1530–1533
- [13] Hyeon-Deuk K and Prezhdo O V 2011 *Nano Lett.* **11** 1845–1850
- [14] Hyeon-Deuk K and Prezhdo O V 2012 *ACS Nano* **6** 1239–1250
- [15] Franceschetti A, An J M and Zunger A 2006 *Nano Lett.* **6** 2191–2195
- [16] Rabani E and Baer R 2008 *Nano Lett.* **8** 4488–4492
- [17] Califano M 2009 *ACS Nano* **3** 2706–2714
- [18] Baer R and Rabani E 2012 *Nano Lett.* **12** 2123–2128
- [19] Allan G and Delerue C 2006 *Phys. Rev. B* **73** 205423
- [20] Delerue C, Allan G, Pijpers J J H and Bonn M 2010 *Phys. Rev. B* **81** 125306
- [21] Shabaev A, Efros A L and Nozik A J 2006 *Nano Lett.* **6** 2856–2863
- [22] Witzel W M, Shabaev A, Hellberg C S, Jacobs V L and Efros A L 2010 *Phys. Rev. Lett.* **105** 137401
- [23] Silvestri L and Agranovich V M 2010 *Phys. Rev. B* **81** 205302
- [24] Korkusinski M, Voznyy O and Hawrylak P 2010 *Phys. Rev. B* **82** 245304
- [25] Kowalski P, Marcinowski L and Machnikowski P 2013 *Phys. Rev. B* **87** 75309
- [26] Azizi M and Machnikowski P 2015 *Phys. Rev. B* **91** 195314
- [27] Nair G, Geyer S M, Chang L Y and Bawendi M G 2008 *Phys. Rev. B* **78** 125325
- [28] Efros A L and Rosen M 1998 *Phys. Rev. B* **58** 7120